

## MESOSCALE MODELING OF CUBE TEXTURE EVOLUTION DURING HOT WORKING OF ALUMINUM<sup>1</sup>

B. Radhakrishnan and G. Sarma

Computer Science and Mathematics Division, Oak Ridge National Laboratory  
Oak Ridge, TN-37831-6359

### Abstract

Cube bands that survive the hot deformation process are known to serve as nuclei for subsequent cube texture evolution in aluminum during static recrystallization. The grain boundary area between cube and other deformation texture components is reported to be an important microstructural feature that influences the growth of the cube nuclei. This paper presents simulations of cube texture evolution at the mesoscopic length-scale with emphasis on the influence of local microstructural environment on the growth of cube islands after hot deformation. The deformation substructure after hot deformation derived from crystal plasticity based modeling of microstructural deformation is used as input to a Monte Carlo simulation of substructure evolution. The effect of neighboring orientations such as Copper and S on the growth of cube bands is investigated as a function of plastic strain and initial grain size. The simulation results are compared with the predictions of existing analytical models of cube texture evolution in polycrystalline aluminum.

### Introduction

The forming and extrusion characteristics of aluminum sheets are influenced by the volume fractions of cube and other deformation components present. In the production of the aluminum hot band, an intermediate product produced by hot deformation, the objective is to achieve a consistently high volume fraction of the cube component by recrystallization so that the subsequent cold deformation steps involved in sheet making can be designed to produce a balanced and optimized volume fraction of cube and deformation components. Therefore, the evolution of cube texture component during recrystallization following hot deformation is of significant technological interest to the aluminum sheet producers.

It is generally believed that the origin of cube nucleation during recrystallization is the presence of cube bands in the hot deformed microstructure. The cube grains that are present in the pre-deformation microstructure survive the hot deformation process [1-3]. Previous experimental [4] and deformation modeling investigations [5, 6] have shown that the stability of the cube grains during hot deformation is enhanced by the operation of additional non-octahedral slip along {110} slip planes. It has also been shown experimentally in deformed bicrystals of specific orientations that the stored energy of deformation within the cube orientation is lower than in the surrounding deformation components, especially the S component [7]. This is based on the observation that the mean subgrain size is larger and the mean misorientation among subgrains is smaller within the cube grains than in grains of other orientations. In addition, there

---

<sup>1</sup> The submitted manuscript has been authored by a contractor of the U.S. Government under contract No. DE-AC05-00OR22725. Accordingly the U.S. Government retains a non-exclusive, royalty-free license to publish or reproduce the published form of this contribution, or allow others to do so, for U.S. Government purposes.

are experimental investigations that showed that the boundary between the cube band and the S orientation has the potential for forming a special  $\Sigma 7$  tilt boundary ( $38.2^\circ$  rotation about  $\langle 111 \rangle$ ) that possesses a combination of higher mobility and lower boundary energy compared to other general high-angle boundaries [8]. The presence of such boundaries is believed to facilitate the accelerated growth of cube grains to consume the S orientations. Based on the above arguments, an analytical theory has been developed, that predicts the recrystallization kinetics and the formation of cube textures in aluminum alloys [9].

The objective of the present investigation is to develop a detailed understanding of the formation of deformation substructures in polycrystalline aluminum as a function of the initial grain structure. The investigation focuses on the effect of initial grain size, the geometry of the cube grains and the amount of hot deformation on the formation and spatial distribution of various types of grain and subgrain boundaries in the deformation substructure, and how they influence the evolution of the cube grains during recrystallization. The outcome of this research will hopefully help in eliminating some of the empiricism existing in analytical theories of cube texture formation. The computational approach described in this paper makes use of the results of a crystal plasticity based microstructural deformation model that appears in a companion paper in this volume [10].

### **Computational Approach**

The deformation substructure after hot deformation derived from crystal plasticity based modeling of microstructural deformation is used as input to a Monte Carlo simulation of substructure evolution. The deformation modeling provides a quantitative description of the crystallographic orientation and the stored energy of deformation in each volume element situated in the microstructure. The first step in applying the results to the mesoscale recrystallization simulations is to construct a deformation substructure that captures the heterogeneity of deformation as depicted by the deformation model.

#### Generation of Substructure

For this purpose, it is assumed that the deformation substructure is made up of a collection of well-defined subgrains within each volume element. The mean subgrain size,  $d$ , and the mean misorientation among subgrains in each element,  $\Delta\omega$ , depend on the stored energy per unit volume in the element,  $H$ , according to [11]

$$H = \frac{\gamma_0}{2d} \left[ \frac{\Delta\omega}{\omega^*} \left( 1 - \ln \frac{\Delta\omega}{\omega^*} \right) \right] \quad (1)$$

where  $\gamma_0$  is the specific energy of a high-angle boundary, and  $\omega^*$  is the misorientation limit for low-angle boundaries taken as  $15^\circ$ . It is assumed that the orientations of the subgrains within each element are scattered around the mean orientation,  $\omega$ , of the element. In the current simulations, the mean subgrain size within the elements is assumed to be constant, and variations in  $H$  among elements generates a subgrain structure with varying subgrain misorientations within each element according to eqn. (1). The stored energy of deformation within each element is calculated as,

$$H = \sum \Delta\tau_{cr} \Delta\gamma \quad (2)$$

where  $\Delta\tau_{cr}$  is the slip system strength and  $\Delta\gamma$  is the increase in the effective slip system accumulated shear in each element during each deformation step. The basis for using eqn. (2) for the stored energy is the assumption that the incremental area in the stress-strain curve of each element arising from the incremental stress and incremental is due to the hardening provided by the increased dislocation density in the element.

The substructure generation step involves the mapping of the substructure information from the finite element mesh that has undergone a shape deformation to regular set of lattice points used in Monte Carlo (MC) simulations. It is assumed that each finite element has the set of  $n_x \times n_y \times n_z$  regularly spaced lattice sites on a cubic lattice where the number of sites  $n_x$ ,  $n_y$  and  $n_z$  in the x, y and z directions is proportional to the element size in three directions after deformation. The MC simulations were carried out using two-dimensional (2-D) sections of the finite element mesh in the RD-ND (x-z) plane, for specific y sections of interest.

### MC Simulation of Recrystallization

In materials such as aluminum that form a well-defined subgrain structure during deformation, the recrystallization during subsequent annealing involves the heterogeneous evolution of the subgrain structure driven by local differences in the subgrain sizes, subgrain boundary energies and mobilities. A MC technique is used to evolve the deformation substructure extracted from the deformation modeling. The details of the simulation algorithm can be found elsewhere [12]. Essentially, the technique involves visiting the various grain boundary sites, calculating the local energy of the site and its neighborhood before and after a proposed flip of the orientation of the site to that of one of its nearest-neighbors, and executing the flip based on certain probability rules. In the current algorithm, the total energy of the site is calculated as

$$E = \sum_{j=1}^m \gamma(S_i, S_j) (1 - \delta_{S_i, S_j}) \quad (3)$$

where  $S_i$  is the orientation of the site visited,  $S_j$ 's are the orientations of the nearest-neighbor sites,  $\gamma$  is the relative energy of the boundary between  $S_i$  and  $S_j$  and  $\delta$  is the Kronecker delta function. The flipping probability is based on

$$p(S_i, S_j) = \begin{cases} 1 & \Delta E \leq 0 \\ \exp\left(\frac{-\Delta E}{kT}\right) & \Delta E > 0 \end{cases} \quad (4)$$

where  $\Delta E$  is the energy difference due to attempted flip,  $k$  is Boltzmann constant and  $T$  is the lattice temperature. Since the presence of a range of boundary misorientations results in boundaries with different energies and mobilities, the total time of visit to a boundary site is scaled according to [12]

$$N_{MCS}^{\mu\gamma} = N_{MCS} \frac{\mu\gamma}{\mu_{max}\gamma_{max}} \quad (5)$$

where  $N_{MCS}^{\mu\gamma}$  is the simulation time for a given boundary site with energy  $\gamma$  and mobility  $\mu$  and  $N_{MCS}$  is the simulation time for a boundary site with the maximum values of boundary energy and mobility,  $\mu_{max}$  and  $\gamma_{max}$ , respectively. The boundary energy is a function of the misorientation, usually represented by the Read-Schockley relationship [11].

$$\gamma = \begin{cases} 0 & \omega = 0 \\ \gamma_0 \frac{\omega}{\omega^*} \left\{ 1 - \ln \left( \frac{\omega}{\omega^*} \right) \right\} & 0 < \omega \leq \omega^* \\ \gamma_0 & \omega > \omega^* \end{cases} \quad (6)$$

the boundary mobility as a function of misorientation is represented by the empirical equation [13]

$$\mu = \mu_0 \left[ 1 - \exp - c(\Delta\omega)^3 \right] \quad (7)$$

where  $c$  is an empirical constant. The above analytical equations for boundary energy and mobility are valid only for general boundaries and low angle boundaries. However, for coincidence site lattice (CSL) boundaries whose misorientations are represented by unique axis-angle pairs, the boundary energy as a function of the misorientation angle goes through minima at these locations, with corresponding maxima in the boundary mobility. In aluminum one such special boundary is the  $\Sigma 7$  boundary characterized by a  $38.2^\circ$  rotation about  $\langle 111 \rangle$  axis. Other special boundaries involving  $\langle 111 \rangle$  rotation axis include the  $\Sigma 13$  and  $\Sigma 19$  boundaries. Recent molecular dynamics simulations (MD) have yielded the relative boundary energy mobility for these special boundaries [14].

In the current simulations, the boundary properties are calculated based on the boundary misorientation using eqns. (6) and (7) for those boundaries whose rotation axis is different from  $\langle 111 \rangle$ . For  $\langle 111 \rangle$  rotated misorientations, the boundary properties are obtained from molecular dynamics results. In reality, there are many boundaries whose misorientations deviate slightly from the exact CSL orientations. The extent of such deviation is calculated using Brandon's criterion [15] according to which the angular deviation within which the CSL properties are exhibited is given by  $15.0/\Sigma^{-1/2}$ . If the Brandon's criterion is satisfied, then the mobility and energy are calculated by interpolating the molecular dynamics data. If not, the properties are calculated using eqns. (6) and (7).

## Simulations

Deformation substructures following hot deformations of 50% and 75% were extracted from deformation simulation results for the following initial microstructures:

1. microstructure consisting of a band of cube-oriented grain surrounded on both sides by a grain structure,
2. microstructure consisting of a cube-oriented grain in the form of a rectangular parallelepiped surrounded by a grain structure,
3. microstructure consisting of a spherical grain of cube orientation embedded in a grain structure,
4. coarse grained microstructure in which a few grains were assigned the cube orientation, and
5. fine grained initial microstructure in which a few grains were assigned the cube orientation,

In all of the above cases, the remaining grains in the initial microstructure were randomly assigned the four crystallographic variants of the S orientation (S1 to S4) and the two crystallographic variants of the Copper orientation (C1 and C2). For the first three cases, the midsection in the transverse direction (TD) was chosen for the MC simulations. For cases 4 and 5 two TD sections were considered, one having the cube grains near the top and bottom edges of the simulation domain, and the other having the cube grains in the interior of the simulation domain. For the 50% deformation case, the size of the simulation domain was  $1280 \times 320$  sites, which corresponds to aspect ratio of 4:1 in the RD-ND plane. For the 75% deformation case the size of the simulation domain was  $2560 \times 160$  sites, corresponding to an aspect ratio after deformation of 16:1 for the RD-ND sections. A constant subgrain size of  $0.4 \mu\text{m}$  was assigned to each site, and the mean misorientation among subgrains in each element was calculated using eqn. (1). For the 75% deformation case, a total of 500 sites at each end of the simulation domain in the RD were skipped during the recrystallization simulations, in order to reduce the simulation domain size and focus on regions in the immediate vicinity of the cube grains. For the 50% deformation case, all the sites in the RD were included in the simulation.

## Results and Discussion

The main objective of the recrystallization simulations is to investigate the evolution of the cube-oriented grains during recrystallization for the various starting deformation structures described previously. The orientation of each site initially represented as three Euler angles was converted to axis-angle pairs, and the rotation angle was used to generate contour plots to represent the recrystallized grain structure. Since the cube orientation is characterized by a small rotation angle, the cube-oriented grains appear the darkest in the recrystallized grain structures shown. The lighter shades represent orientations of sites belonging to the S and Copper orientations.

### Recrystallization Following 50% Deformation

Figure 1 shows the deformed grain structure for a deformation of 50 % for the band, block and sphere cases and the corresponding recrystallized microstructures.

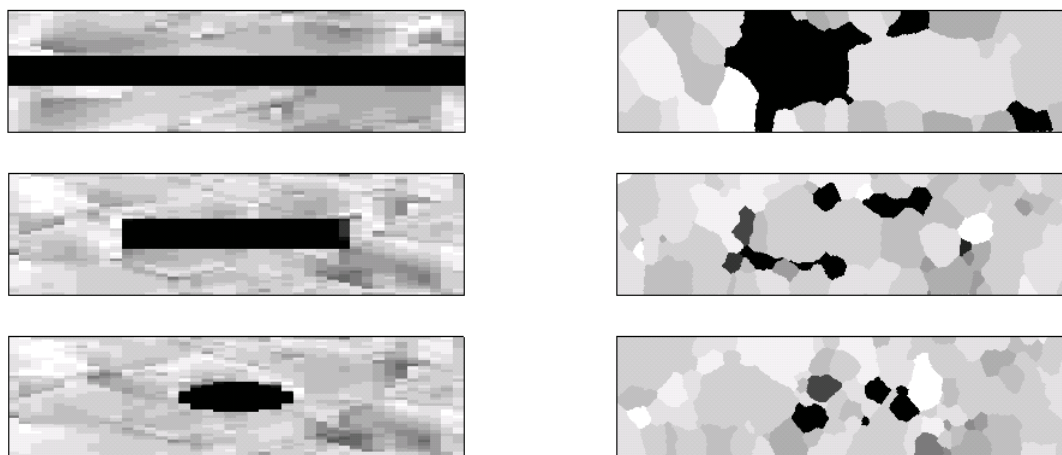


Figure 1. Microstructures after 50% hot deformation (left) and the corresponding recrystallized microstructures (right). The cube orientations appear dark.

It can be seen from figure 1 that the growth characteristics of the cube grain during recrystallization in the three cases are significantly different. In the case of the cube band, only a portion of the cube band served as an effective nucleation site while a major portion of the initial band is consumed by the growth of a non-cube grain. In the case of the block and sphere,

only traces of the initial cube grains remain. In the case of the cube block, the spatial location of some of the cube islands in the recrystallized condition is significantly far away from the location of the cube block, indicating that the cube regions grew initially during recrystallization, but were consumed by another non-cube grain during later stages of recrystallization. A similar sequence of events apparently occurred for the case of the sphere, although the remaining cube islands are quite close to the initial cube grains, indicating less growth compared to the block case.

A close examination of the grain structure in the recrystallized microstructures also indicates that the non-cube grains that grow and consume the cube grains are rather large, indicating abnormal growth. Such a growth is aided either by a large driving force or a high boundary mobility or both. This aspect of grain growth will be discussed later.

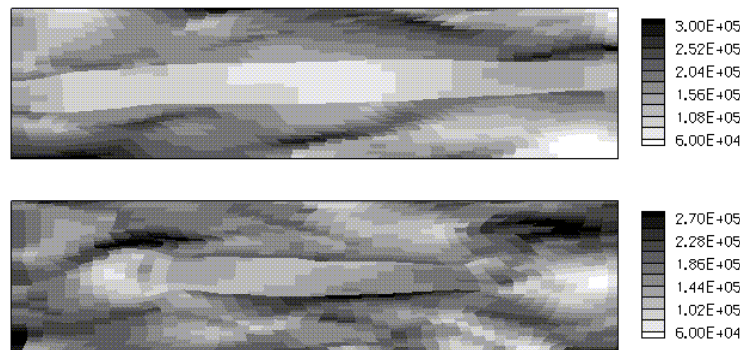


Figure 2. Stored energy distribution ( $\text{J/m}^3$ ) after 50% hot deformation for a grain structure containing cube band (top) and cube block (bottom).

The underlying reason for the difference in the evolution of the central cube grain in the above three cases is because of the difference in the stored energy distribution. Figure 2 shows the stored energy distribution for the microstructures containing the cube band and cube block. In the case of the cube band, the stored energy within the band is clearly lower than in the surrounding microstructure. Therefore, there should be driving force for the cube band to grow and consume the surrounding grain structure. However, it appears that the cube band has been consumed on the right side by another growth front that originated in the surrounding grain structure. The reason that this occurred is due to the local heterogeneity present in the deformation substructure. As described previously, the extraction of the deformation substructure involves the assumption of a constant size for the subgrains in all the volume elements and then calculating the misorientation among subgrains within each element using eqn. (1). This means that the mean subgrain misorientation will be higher in regions with higher stored energy per unit volume. Since the subgrain mobility increases with misorientation, these regions will recover faster than the regions with lower stored energy. It is therefore possible that after a certain time the total grain boundary energy per unit volume in these regions will become lower than in the surrounding regions that initially had lower stored energy. If the rate of recovery is fast enough to cause this reversal in the direction of the driving force before significant interface migration occurs, then the interface will move from a region with an initial high stored energy to a region with initial low stored energy. Close examination of figure 2 shows that there are high-energy bands in non-cube regions in the vicinity of the cube grain. The growth fronts originated in these regions and consumed the cube grain before the cube grain had the chance to grow out. In the case of the cube block, the stored energy within the block is lower than in the surrounding grain structure, especially in the midsection. However, just outside the two ends of the cube block there are regions with significantly lower stored energy.

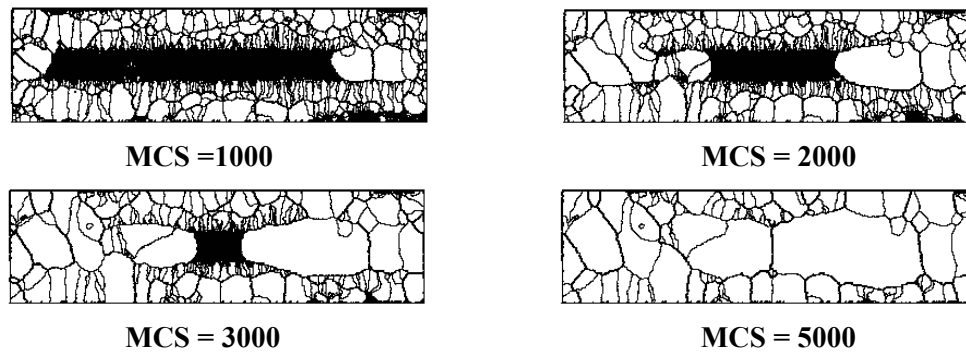


Figure 3. Temporal evolution of the recrystallization microstructure for the cube band after a 50% hot deformation.

The temporal evolution of the recrystallized grain structure is shown in figure 3. The grain boundaries indicated in bold lines in figure 3 are high angle boundaries with a misorientation angle of greater  $15^\circ$ . They also include the special CSL boundaries ( $\Sigma 7$ ,  $\Sigma 13$  and  $\Sigma 19$  boundaries) that did form in the as-deformed grain structure. The grain boundaries that are indicated by light lines are small angle grain boundaries. The same line style is used in all of the subsequent microstructures. After a simulation time corresponding to 1000 Monte Carlo steps (MCS), the cube band has grown out to consume the surrounding grains. The outward migration of the cube band results in the formation of several low angle boundaries that are almost perpendicular to the high angle growth front. At the same time we can see the formation of several large grains surrounded by high angle boundaries in both the right and left extremes of the cube band. Comparing the grain structure with the stored energy distribution shown in figure 2, it can be seen that these growth fronts originate in the high stored energy bands situated at these locations, indicating the operation of a rapid recovery process as indicated previously. These growth fronts consume the cube band from both directions including a portion of the cube band that grew out initially.

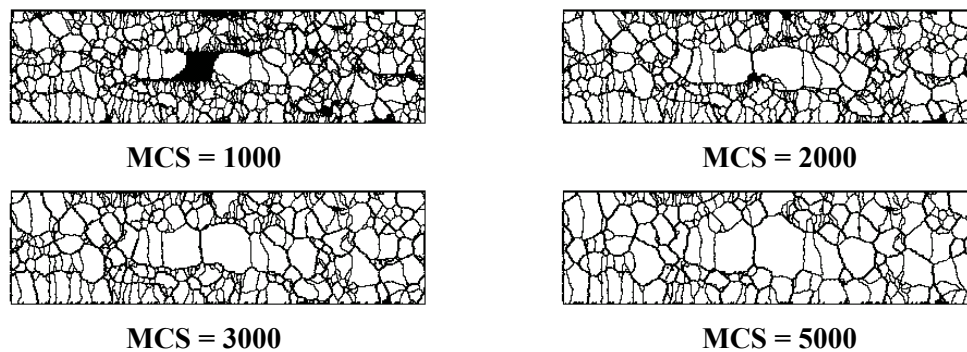


Figure 4. Temporal evolution of the recrystallization microstructure for the cube block after 50% hot deformation.

Figure 4 shows temporal evolution of the recrystallized grain structure for the microstructure containing the cube block. After 1000 MCS, there is a clear indication of the cube block growing out to consume the surrounding grains, especially in the upper middle portion of the cube block that had the lowest stored energy. As in the case of the cube band, the growth front drags with it some low angle boundaries that are almost vertical to the cube edge. However, there are also growth fronts that originate at both ends of the cube block. Comparing the grain structure with the stored energy distribution shown in figure 2, it is clear that these growth

fronts correspond to the migration of a non-cube interface into the cube from lower stored energy regions in the non-cube regions just outside the edges of the cube block.

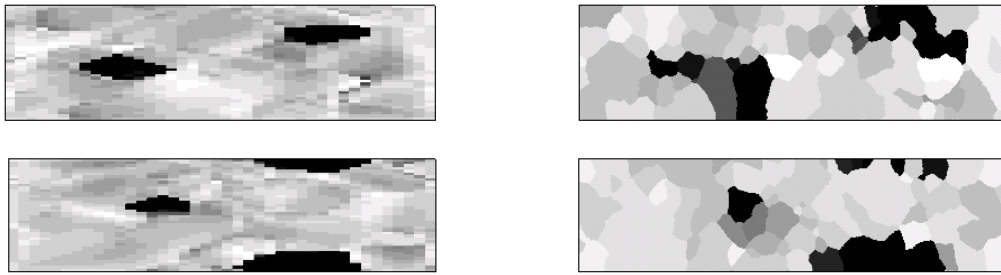


Figure 5. Deformation structure (left) and recrystallized grain structure (right) for the fine grained grain structure with assigned cube grains.

The deformation microstructure and the corresponding recrystallized microstructure are shown in figure 5 for the fine grained microstructure in which a few grains were assigned the cube orientation prior to the deformation. The essential difference between this case and the ones shown previously is that the size of the cube grains is comparable to the size of the surrounding grains in the initial microstructure. The top figures correspond to the TD section where the cube grains are present inside the simulation domain while the bottom figures correspond to the TD section where the cube grains are on the top and bottom surfaces of the simulation domain. It is seen from the top figure that both the interior cube grains grow during recrystallization, although growth fronts originating in the non-cube regions consumed the cube during the latter stages of recrystallization, similar to the cube band and cube block cases discussed previously. The behavior of the surface grains shown in the bottom figures is quite similar.

In both the coarse and fine grained microstructures, the cube grains were somewhat unstable compared to the cube band and the cube block [10], that resulted in the nucleation and growth of grains that are significantly rotated from the exact cube orientation, as seen in figure 5. Also since the stored energy within the cube grains in these two cases were higher than in the surrounding grains [10], it is possible that the nucleation mechanism involved a rapid recovery by subgrain growth within the cube grains causing the stored energy within the cube to become lower than in the surrounding grains.

### Recrystallization Following 75% Deformation

This section describes the details of substructure formation and evolution during recrystallization of the deformation substructure formed after a 75% deformation. As previously mentioned, 500 lattice sites from each end of the simulation domain (corresponding to about 8 finite elements) were skipped in the MC simulation of recrystallization in order to reduce the size of the simulation domain and focus on the regions in the immediate vicinity of the cube grains.



Figure 6. Deformation structures produced after 75% deformation for the cube band, sphere and cube block cases

Figure 6 shows the deformation substructure for the cube band, sphere and block cases plotted as a contour map of the rotation angle for each lattice site. As in the 50% deformation case, the cube grains appear dark and the lighter shades represent the orientations of the sites belonging to the S and cube grains after deformation. It is interesting to note that sites with low rotation angles exist in regions far away from the cube grains, indicating that these orientations formed as a result of the deformation process. However, the evolution of these cube grains was not simulated because these regions formed a part of the end zone that was skipped in the MC simulations.

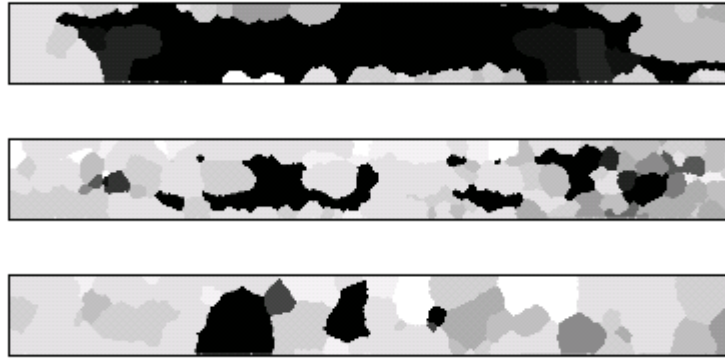


Figure 7. Recrystallized grain structures following 75% deformation showing the evolution of the initial cube grains for cube band (top) and cube block (middle) and sphere (bottom)

The distribution of the cube and non-cube grains in the recrystallized grain structures shown in figure 7 exhibit almost all of the features associated with the evolution of the cube grains described for the 50% deformation case. In the case of the cube block, the growth occurred prior to its consumption by a non-cube growth front, as indicated by the spatial locations of the remnant cube grains. The spherical cube grain did manage to grow at the extreme left end although it was almost eliminated at other locations. There is also an indication of the nucleation and growth of a rotated cube component. It should be noted that the stored energy within the cube was only marginally lower than the surrounding grains at certain locations {10}. However, the final volume fraction of the cube band after recrystallization in this case is significantly higher than that for the 50% deformation case. This is probably due to the elimination of the end regions that successfully nucleated non-cube grains that grew into the cube regions for the 50% deformation case.

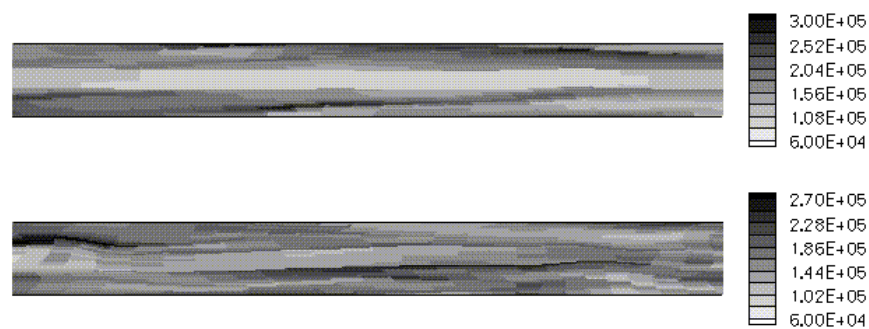


Figure 8. Stored energy distribution for the cube band (top) and cube block (bottom).

Figure 8 shows the stored energy distributions for the cube band and cube block cases after 75% deformation. The stored energy within the cube band and the block continue to be lower than in the surrounding grain structure, which facilitates the initial outward growth of the cube

grains. However, even with the exclusion of the end elements, there still exist growth fronts in the non-cube regions that ultimately consume part of the cube grain in the case of the cube band. For the cube block, the stored energy difference between the cube and the surrounding grains is slightly smaller than for the cube band. Also, there is a high stored energy band adjacent to the cube band that recovered rapidly and set up a growth front into the cube grain.

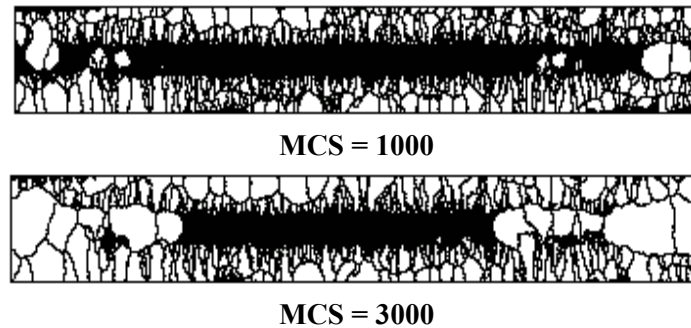


Figure 9. Temporal evolution of the cube band during recrystallization

Figure 9 shows the temporal evolution of the cube band during recrystallization. Note the formation of growth fronts at the extreme ends of the band that start to consume the cube band while the lateral edges of the cube band grow outward to consume the non-cube grains. An interesting new aspect of microstructural evolution in this case is the formation of abnormal growth fronts inside the cube band. These growth fronts apparently block the advance of the non-cube growth fronts into the cube band from the sides. This can be seen by comparing the microstructure after 3000 MCS with the cube grain shown in figure 7. Note that the abnormal growth fronts within the cube band have a lighter color compared to the bulk of the cube grain, indicating significant misorientation between the two regions.

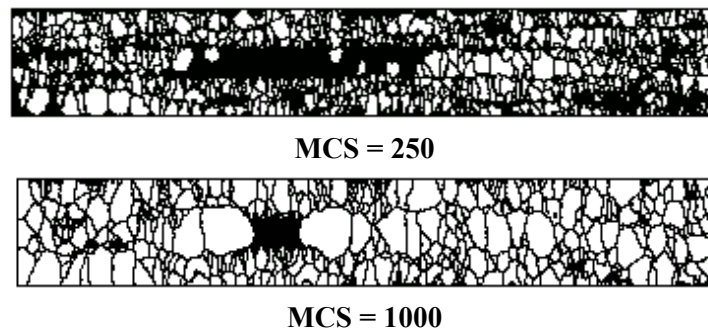


Figure 10. Temporal evolution of recrystallization for the cube block.

Figure 10 shows the temporal evolution of the recrystallized microstructure for the cube block. The cube block appears to get consumed from the right hand side where the stored energy in the cube is either equal to or slightly higher than the stored energy outside, as seen in figure 8. Portions of the cube block manage to grow outward and survive the consumption from the non-cube band. The cube block is also consumed from the left hand side although to a lesser extent by a growth front that seems to originate at the top edge of the cube band.

The results shown above indicate that there are two distinctly opposing mechanisms that control the evolution of the cube grains. First, the cube grains tend to grow outward and consume the subgrains belonging to the S and Copper deformation components, thereby tending to increase its volume fraction. This is driven mainly by the lower stored energy within the cube grain as compared to the surrounding S and Copper oriented grains. As the interface between the cube

and non-cube grains migrates outward it drags the low angle boundaries behind it, thus producing a number of columnar grains in its wake. At the same time, a discontinuous growth front develops in regions of high stored energy in the vicinity of the cube band, probably by an accelerated recovery process which migrates inside the cube and consumes it preferentially accessing the central portion of the cube grains that have a large number of low angle boundaries.

The microstructural evolution of the cube grains is largely influenced by the assumption of the deformation substructure. In the simulations so far, it has been assumed that the mean subgrain size is constant for all elements, while the element-to-element variation in stored energy produced corresponding differences in the mean misorientation among subgrains belonging to an element. However, it is also equally justified in assuming that the mean misorientation among subgrains is constant for all elements, which would produce element-to-element variation in the mean subgrain size.

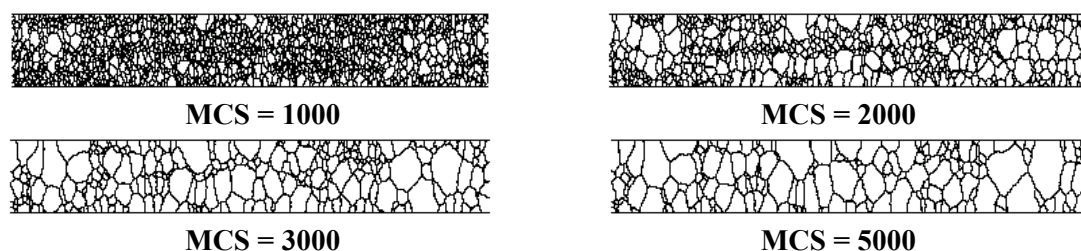


Figure 11. Microstructural evolution during recrystallization of cube block, assuming that the deformation substructure has constant subgrain misorientation

Figure 11 shows the temporal evolution of the deformation substructure for the cube block, where the deformation substructure is constructed by assuming that the mean misorientation among subgrains is constant for all elements, and the element-to-element variation in subgrain size is calculated based on the corresponding stored energy. The subgrain structure is again seen to evolve heterogeneously, with the interface between the cube block and the outer regions moving in such a way as to either consume or grow the cube orientation. However, there is no indication of the cube block being consumed by growth fronts in the horizontal direction as seen figure 10. The distribution of the cube grains after recrystallization in this case is shown in figure 12. The spatial location of the cube grains has no resemblance to the one seen in figure 7.

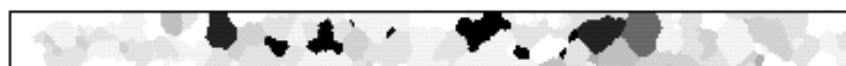


Figure 12. Spatial distribution of cube oriented grains after recrystallization for the substructure evolution shown in figure 11.

One of the problems in representing the deformation substructure based on the assumption of constant subgrain misorientation is that it is not possible to come up with a unique value of mean subgrain size for a given element. Since there is an inherent size distribution in a grain structure, there will always be situations where a grain of a smaller size will be situated in the lower stored energy region with a significantly bigger grain situated next to it in the higher stored energy region. Under such conditions, the local migration direction of the interface will be from a high to a low energy region, although in an average sense the interface should migrate from a low energy to a high-energy region. Such local fluctuations are particularly important when the average stored energy difference between the two regions is small. On the

other hand, if the substructure is created on the basis of a constant subgrain size within the elements with the misorientation among subgrains allowed to vary based on the local stored energy, it is possible to eliminate the statistical variation in subgrain size, by assuming an initial grain size of 1.0, which means that that each lattice site is a subgrain. However, such a grain structure is not topologically correct. Also, under these conditions it is possible for a region that initially has the higher stored energy to recover quickly by subgrain growth (higher subgrain misorientation leads to higher subgrain mobility) which results in the stored energy becoming lower than the surrounding regions, causing the interface migration to change direction. Note that such a reversal in the relative magnitudes of the stored energy is not possible for the case of constant boundary misorientation [16].

In a real deformation substructure, the mean subgrain size and subgrain misorientation within a grain of a given initial orientation depend on the nature of the local deformation, the total number and types of dislocations that are produced and the evolution of the dislocation substructure. The constitutive equations used in the crystal plasticity formulation are continuum equations, although they are applied to a grain structure. Although the constitutive equation allows for the orientation dependence of crystallographic slip and the evolution of slip system hardness, it does not include the atomistic mechanisms involved in the formation, multiplication and rearrangement of dislocation. Thus, even though the slip system hardness and its evolution with plastic strain can capture the yield strength of the material, and therefore, the mean subgrain size, it does not provide a direct measure of the subgrain misorientation. On the other hand lower length scale simulations of discrete dislocation dynamics cannot handle the large plastic strains encountered in thermo-mechanical processing. Therefore, realistic modeling of deformation substructures is still a significant challenge to the modeling community.

The evolution of the deformation substructures is also very sensitive to the boundary properties. Although the current simulations do account for the formation of special CSL boundaries, and realistic properties for such boundaries have been extracted from MD simulations, there are still significant ambiguities in the choice of boundary properties. For example, if a special boundary deviates slightly from the exact CSL position, although it satisfies the Brandon's criterion for the given boundary type, it is not clear how to obtain a realistic estimate of the properties of such a boundary. This is because the deviation from the exact CSL position can be either in the rotation angle or the rotation axis or both, and currently there are no rigorous ways to estimate the change in boundary properties due to these deviations. Another ambiguity in the choice of the grain boundary properties arises because it is not possible to include in the model whether a given CSL boundary is of the tilt or the twist type. It is well known that the high mobility and low energy associated with the  $\Sigma 7$  boundaries in aluminum apply only to tilt boundaries and not for twist boundaries.

## **Summary and Conclusions**

The deformation substructure in hot-deformed grain structures containing initial cube-oriented grains of different geometries was extracted from the stored energy and crystallographic orientation information provided by a microstructural deformation model based on crystal plasticity approach. The stored energy of deformation was assumed to be equal to the surface energy of the subgrains that form during hot deformation. The heterogeneity in the deformation substructure was captured in the model by assuming that the subgrain size within each volume element is constant, which provides an element-to-variation in subgrain misorientation based on the stored energy. The subgrain structures were evolved using a MC technique, and using realistic properties for the subgrain boundary energy and mobility, including all the CSL boundaries based on a  $\langle 111 \rangle$  axis of rotation.

The simulations showed that when the size of the initial cube grains were much larger than the sizes of other grains in the microstructure (cube band, block and sphere cases) orientations very close to perfect cube grew by consuming the surrounding non-cube orientations. However, rapid recovery in high stored energy regions adjacent to the cube set up discontinuous growth fronts that consumed portions of the cube, thus resulting in insignificant overall growth of the cube orientation. When the size of the initial cube grains was comparable to the size of the other grains (fine and coarse grained grain structures with assigned cube grains) the nucleation growth probably involved a rapid subgrain growth within the cube aided by the high stored energy within the cube followed by the discontinuous growth of rotated cube orientations.

The simulation results are quite sensitive to the assumptions used in the generation of the deformation substructure. Further research is required to eliminate the ambiguities involved in the substructure generation, as well as in the choice of boundary properties.

### Acknowledgements

Research sponsored by the Office of Basic Energy sciences, U.S. department of Energy under contract DE-AC05-00OR22725 with UT-Batelle, LLC.

### References

1. H.E. Vatne, T. Furu and E. Nes, "Nucleation of Recrystallized Grains from Cube bands in Hot Deformed Commercial Purity Aluminium," Mater. Sci. Tech. Ser., 12 (1996), 201-210.
2. O. Daaland, and E. Nes, "Origin of Cube Texture during Hot Rolling of Commercial Al-Mn-Mg Alloys," Acta mater. 44 (1996), 1389-1411.
3. O. Daaland and E. Nes, "Recrystallization Texture Development in Al-Mn-Mg Alloys," Acta mater 44 (1996), 1413-1435.
4. C. Maurice and J.H. Driver, "High Temperature Plane -Strain Compression of Cube Oriented Aluminum Crystals, Acta mater met. 41 (1993) 1653-1664.
5. C. Maurice and J.H. Driver, "Hot Rolling Textures of FCC Metals," Acta mater. 45 (1997), 4639-4649.
6. G. Sarma, B. Radhakrishnan and T. Zacharia, "Modelling the Deformation of Face Centered Cubic Crystals to Study the Effect of Slip on {110} Planes," Modelling Simul. Mater. Sci. Eng. 7(199) 1025-1043.
7. M.C. Theyssier and J.H. Driver, "Recrystallization Nucleation Mechanism along Boundaries in Hot Deformed Aluminum Bicrystals," Mater Sci Eng A, 272 (1999), 73-82.
8. M.G. Ardakani and F.J. Humphreys, "The Annealing Behavior of Deformed Particle-containing Aluminum Single Crystals," Acta mater met. 42 (1994), 763-780.
9. H.E. Vatne et al. "Modeling the Recrystallization after Hot Deformation in Aluminum," Acta mater. 44 (1996), 4463-4473.
10. G. Sarma, B. Radhakrishnan and T. Zacharia, "Application of Mesoscale Finite Element Simulations to the Study the Evolution of Cube Texture during Hot Deformation of Aluminum," this volume.

11. F.J. Humphreys and M. Hatherly, Recrystallization and Related Annealing Phenomena, (Oxford, UK: Elsevier Science Ltd., 1995), 62.
12. B. Radhakrishnan and T. Zacharia, "On the Monte Carlo Simulation of Curvature-Driven Growth," Modelling Simul. Mater. Sci. 10 (2002), 227-236.
13. A.D. Rollett and E.A. Holm, "Abnormal Grain Growth – The Origin of Recrystallization Nuclei?" Proceedings of ReX'96, the Third International Conference on Recrystallization and Related Phenomena, ed. T.R. McNelley (Monterey, CA: Monterey Institute of Advanced Studies), 31-41.
14. M. Upmanyu et al., "Boundary Mobility and Energy Anisotropy Effects on Microstructural Evolution during Grain Growth," Interface Science, 10 (2002), 201-216.
15. D.G. Brandon, "The Structure of High-Angle Grain Boundaries," *Acta met.* 14 (1966), 1479-1484.